

Use of fine particle quartz sand for AAC production: model study by *in situ* X-ray diffraction and NMR

ABSTRACT: In order to clarify important factors which govern the tobermorite formation in hydrothermal reaction, the effects of quartz particle size and water content were investigated for simplified model systems by *in-situ* XRD and Si-NMR. Although the reaction time was largely dependent on the quartz particle size, the average Ca/Si in non-crystalline C-S-H at the time that either tobermorite or semi-crystalline C-S-H start to be formed (T0) was nearly identical for all samples. The importance of molar ratio Ca/Si as well as the silicate chain length in non-crystalline C-S-H was suggested. Tobermorite can be synthesized even in the systems with large w/s and fine quartz. It was suggested that lower calcium and/or silicate ion concentration in the solution phase is important for tobermorite formation.

KEY WORDS: *in-situ*, XRD, NMR, particle size

1. Introduction

It is well known that the quality of silica source in the starting material of AAC largely affects the mechanical properties of the final product. Quartz sand is one of the most widely used silica sources for the AAC manufacturing. Properties of natural quartz sand such as particle size, amount of impurity and crystallinity vary significantly according to its producing area. Differences in these properties would result in the quality and quantity of tobermorite formed in the AAC, which largely affect the physical properties of AAC [1]. From the economical point of view, however, it is very important to be able to utilize wide variety of silica sources for the AAC production. Thus, investigation of the tobermorite formation process from various silica sources would provide important information for AAC industry.

X-ray diffraction (XRD) and solid state NMR have been powerful tools for characterization of calcium silicate hydrate for decades. Recently we have developed synchrotron-based *in situ* XRD system for the investigation of reactions under autoclave condition, and the formation process of tobermorite from cement-based starting materials has been successfully observed [2-4].

In the present study, we applied this method to simplified high-purity (reagent-based) model system, and investigated the effect of quartz particle size and water content in starting mixtures on the tobermorite formation, in order to find a way to use fine particle quartz sand as a starting material of AAC. Characterization of non-crystalline C-S-H phase just before the tobermorite formation was also conducted by solid state Si-NMR.

2. Experimental

2.1. Materials and sample preparation

The starting materials were mixtures of 56 wt.% natural quartz sand (purity > 99.4%) and 44 wt.% quicklime (99.9%, Kanto Kagaku). The molar ratio of Ca/Si in these mixtures was 0.84, which is nearly identical to stoichiometric value of tobermorite. Three types of quartz sand having different particle size distributions were used; average particle size of 2.2 micron (Q-A), 4.2 micron (Q-B) and 25 micron (Q-C). The starting mixtures were fully mixed in the presence of water. The water-to-solid ratio (w/s) was either 1.5 or 1.7 by weight, except for the mixtures with fine quartz sand, Q-A, for which the slurries with the w/s of 3.0, 6.0 and 9.0 were also prepared. After held at 50°C for more than 2 h, about 0.5 g of slurry sample was set in an originally made autoclave cell for *in situ* XRD measurement, as described in the following section. Non-crystalline C-S-H (n-C-S-H) samples for Si-NMR were prepared using the same autoclave cell, by stopping the reaction just before the tobermorite formation. The n-C-S-H samples together with residual quartz were taken out from the cell, and immersed into acetone to avoid further reaction, and then dried in vacuum at room temperature.

2.2. *In situ* XRD measurement

Slurry sample was set in the autoclave cell for *in-situ* XRD measurement. Details of the autoclave cell are described elsewhere [2-4]. *In situ* XRD measurements were carried out at the BL19B2 beamline of SPring-8, using an X-ray energy of 30 keV. A schematic diagram of the experimental set-up is shown in Fig. 1. The temperature of the cell was elevated to 100°C at a rate of 2°C/min and held at 100°C for 15 min. During this period, the air inside the

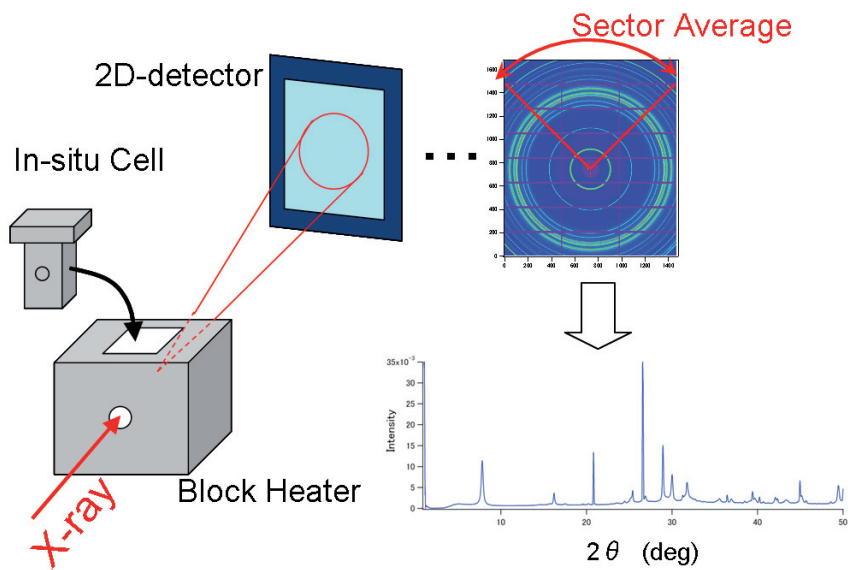


Fig. 1. Schematic of experimental set-up.

cell was removed by opening a pressure release valve for a few seconds. After the steam pressure was built up again at 100°C, the first XRD measurement was conducted. After 15 min at 100°C, the temperature was elevated again to 190°C at a rate of 1°C/min, and then held at 190°C for typically 9 h. During this process, the XRD measurements were conducted at a time interval of 3 min. using a photon-counting pixel array detector, PILATUS-2M (DECTRIS). Upper part of the circular signal (from -45 to 45 deg) was sector-averaged to obtain one-dimensional diffraction pattern. Peak intensities were determined by peak areas after being normalized with the transmitted beam intensities. The reaction times shown on the horizontal axes of the figures are defined as the times at the beginning of the corresponding measurement cycle, and the time zero is defined as the time at which the temperature started to be elevated from 100 to 190°C.

2.3. $^{29}\text{Si-NMR}$ measurement

$^{29}\text{Si-NMR}$ spectra were acquired by Bruker Biospin DSX400 spectrometer (9.4 T) using DD-MAS mode (spinning frequency: 4.5 kHz). Number of scans was 800 with a recycle delay of 100 s. Peak areas of Q1, Q2 and Q3 components were determined by curve-fitting using gaussian/lorenzian mixed function, and silicate chain length for each sample was estimated [5].

3. Results and discussion

3.1. Effect of quartz particle size

Figure 2 shows a typical in situ time-resolved XRD data set obtained under autoclave condition. The phase evolution during the autoclave is clearly observed. At

the beginning of the autoclaving (at 100°C), quartz and portlandite (hydrated quicklime) were observed. After the dissolution of both constituents, n-C-S-H halo was detected. With the decrease of C-S-H halo, several peaks of tobermorite started to be observed. This type of data set was acquired for each sample.

Time dependences of the intensities of major peaks were obtained from the data set. The intensity curves for samples using Q-A, Q-B, and Q-C, after quartz and portlandite curves were normalization by the intensity at $t = 0$, are compared in Fig. 3. Here, intensity curves from same constituent (e.g. Q(101), Q(100) and Q(110)) are averaged to obtain better statistics. It is clearly shown that the dissolution rate of quartz decrease with increasing quartz particle size. It is interesting that the decrease rate of portlandite also varies according to quartz particle size, indicating that the decline

of portlandite is largely affected by the dissolution of quartz. This may be attributed to the beginning of reaction of silicate ions with calcium. As shown in Fig. 2, n-C-S-H is formed as result of dissolution of quartz and portlandite. When Ca ions in the solution phase are consumed by the formation of C-S-H, further dissolution of portlandite becomes possible. In other words, portlandite cannot be dissolved further unless Ca ions are consumed in some way.

As shown in Fig. 3 (a), tobermorite was not formed in the sample using Q-A quartz, implying that the fine particle quartz cannot be used as a starting material of AAC. Instead, semi-crystalline C-S-H (similar structure to tobermorite but lack of ordering along c axis) was observed. To explain the reason why tobermorite cannot be formed, the chemical state of n-C-S-H just before either tobermorite or semi-crystalline C-S-H (semi-C-S-H) is formed was compared. For all samples, portlandite completely disappeared just before

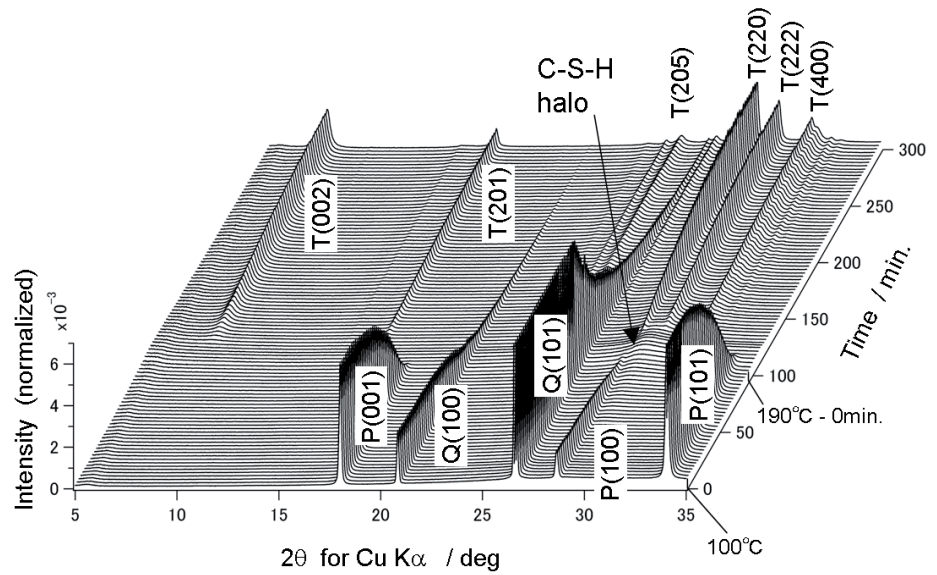


Fig. 2 In situ time-resolved XRD data set for sample using Q-B quartz sand.
Q: quartz, P: portlandite, T: tobermorite

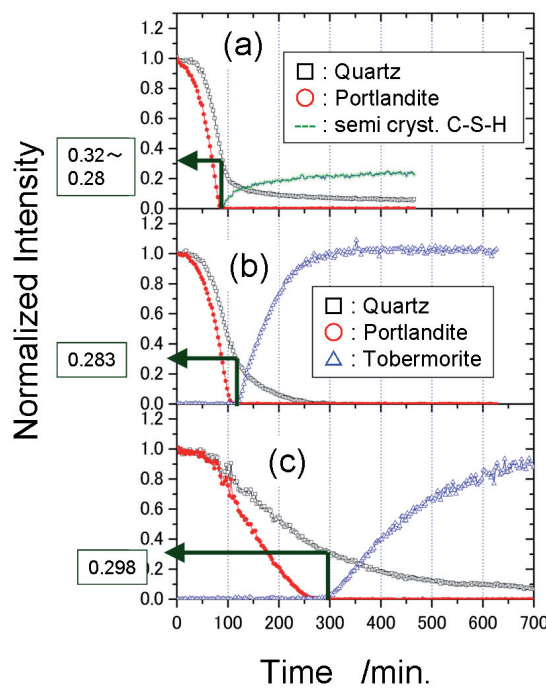


Fig. 3. time dependences of the averaged peak intensities for samples with different quartz size distribution: (a) Q-A, (b) Q-B, (c) Q-C.

either tobermorite or semi-C-S-H started to be formed, while a certain amount of quartz remained undissolved. Amount of the remaining quartz at the time that either tobermorite or semi-C-S-H started to be formed (hereafter, denoted by T0) is shown for each sample in Fig. 3. It is interesting that the amount of the remaining quartz at T0 is nearly identical for all samples, regardless of the absolute value of T0. This suggests that the n-C-S-H start to be transformed to either tobermorite or semi-C-S-H at a certain composition threshold (Ca/Si ratio), assuming that all of the dissolved quartz and portlandite are incorporated in n-C-S-H.

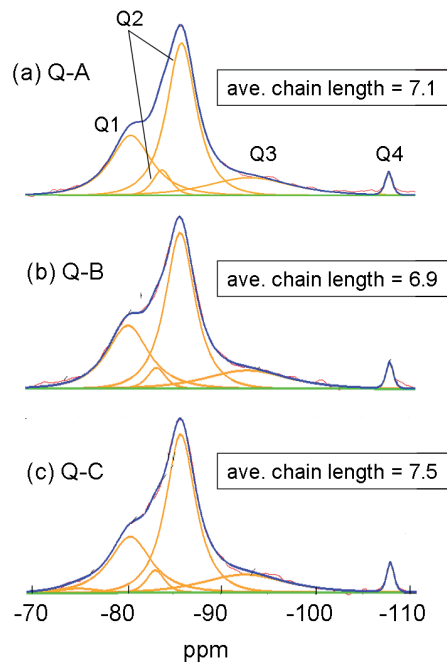


Fig. 4. ^{29}Si NMR spectra for samples with different quartz size distribution: (a) Q-A, (b) Q-B, (c) Q-C.

The chemical state of n-C-S-H at T0 was investigated by Si-NMR. NMR spectra for samples with Q-A, Q-B and Q-C quartz are shown in Fig. 4, together with the estimated average chain length of silica tetrahedra. The spectra did not show clear difference, and the values of average chain lengths showed no clear trend among three samples.

The results described above imply that neither “average” composition nor “average” silicate chain length of n-C-S-H would be a main factor to determine whether tobermorite formation occurs or not. Thus, we assume the “distribution” (or “variation”) of the composition or chain length in the n-C-S-H would be important. The distribution analyses are currently underway in our laboratory.

3.2. Effect of water-to-solid ratio

Effect of water-to-solid ratio (w/s) was investigated for sample with Q-A quartz. Four samples with different w/s were prepared and investigated by in-situ XRD (w/s = 1.7, 3.0, 6.0 and 9.0). The time dependences of the intensities of each constituent are shown in Fig. 5. As described in the previous section, sample with w/s = 1.7 did not show any tobermorite peaks, while other samples with w/s > 3 showed clear tobermorite peaks. To compare the dissolution rates of quartz and portlandite among these samples, an overlay plot of the time dependence of quartz and portlandite are shown in Fig. 6. Surprisingly, quartz dissolution curves are nearly identical to each other. Even though the water content is largely different by a factor of 5, the dissolution rate does not change at all.

The results shown in Fig. 6 indicate that the quartz dissolution rate is predominated by its surface area, and that the dissolution

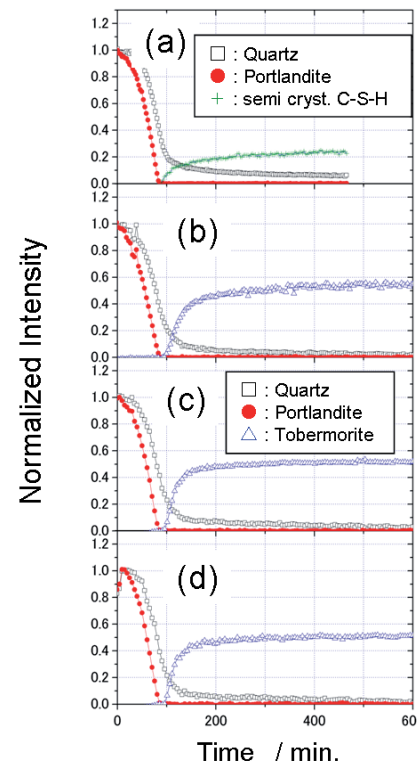


Fig. 5. Time dependences of the averaged peak intensities for samples with different w/s ratio: (a) w/s = 1.7, (b) 3.0, (c) 6.0, (d) 9.0.

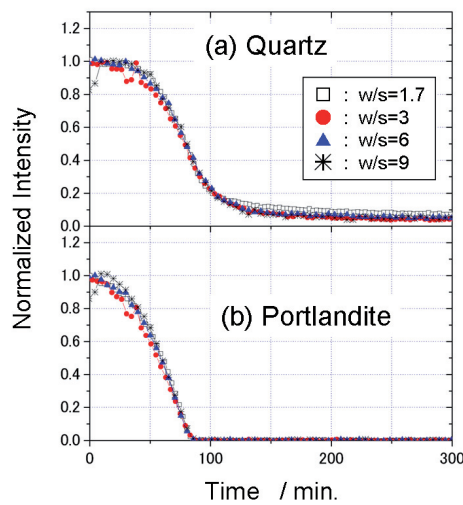


Fig. 6. Overlay plot of time dependences of averaged peak intensities of (a) quartz and (b) portlandite for samples with different w/s.

rate itself does not affect whether tobermorite is formed or not. Moreover, the fact that the time dependences of both quartz and portlandite intensities are identical among these samples implies the Ca/Si ratios of n-C-S-H are also identical among these samples throughout the reaction. Therefore, concentration of Ca and/or Si ions in the solution phase is considered to be an important factor for tobermorite formation.

4. Conclusion

In order to clarify important factors which govern the tobermorite formation in hydrothermal reaction, the effects of quartz particle size and water content were investigated for simplified model systems by in-situ XRD and Si-NMR. Although the reaction time was largely dependent on the quartz particle size, the average Ca/Si in non-crystalline C-S-H at the time that either tobermorite or semi-crystalline C-S-H start to be formed (T_0) was nearly identical for all samples. The importance of molar ratio Ca/Si as well as the silicate chain length in non-crystalline C-S-H was suggested. Tobermorite can be synthesized even in the systems with large w/s and fine quartz. It was suggested that lower calcium and/or silicate ion concentration in the solution phase is important for tobermorite formation.

Acknowledgment

This study was performed with the approval of JASRI (Proposal Nos. 2009B1788, 2009B2015, 2010A1694 and 2010A1831).

Bibliography

- [1] Alexanderson J., 1979. Relations between structure and mechanical properties of autoclaved aerated concrete. *Cem. Concr. Res.* **9**, 507-514.
- [2] Kikuma J., Tsunashima M., Ishikawa T., Matsuno S., Ogawa A., Matsui K., Sato M., 2009. Hydrothermal formation of tobermorite studied by in situ X-ray diffraction under autoclave condition. *J. Synchrotron Radiat.* **16**, 683-686.
- [3] Kikuma J., Tsunashima M., Ishikawa T., Matsuno S., Ogawa A., Matsui K., Sato M., 2010. In situ time-resolved X-ray diffraction of tobermorite formation process under autoclave condition. *J. Am. Ceram. Soc.* **93**, 2667-2674.
- [4] Kikuma J., Tsunashima M., Ishikawa T., Matsuno S., Ogawa A., Matsui K., Sato M., 2010. Formation process of autoclaved lightweight concrete studied by in situ X-ray diffraction under hydrothermal condition. *Bunseki Kagaku* **59**, 489-498.
- [5] Richardson I.G., 1999. The nature of C-S-H in hardened cements. *Cem. Concr. Res.* **29**, 1131-1147.